

Article

Removal of Potassium and Iron in Low Grade Bauxite by a Calcination-Acid Leaching Process

Zhuang Li ^{1,2}, Yijun Cao ^{3,*}, Yuanli Jiang ², Guihong Han ^{1,*}, Guixia Fan ¹ and Luping Chang ¹

¹ School of Chemical Engineering and Energy, Zhengzhou University, Zhengzhou 450046, China; gold1064@126.com (Z.L.); zdhgfgx@zzu.edu.cn (G.F.); changluping1988@163.com (L.C.)

² Research Institute of Henan Energy and Chemical Industry Group, Zhengzhou 450046, China; jyl@zzu.edu.cn

³ Henan Province Industrial Technology Research Institute of Resources and Materials, Zhengzhou 450046, China

* Correspondence: caoyj@cumt.edu.cn (Y.C.); hanguihong@zzu.edu.cn (G.H.); Tel.: +86-371-67781801 (Y.C.); +86-371-6933-7225 (G.H.)

Received: 18 January 2018; Accepted: 16 March 2018; Published: 22 March 2018



Abstract: In order to explore the commercialized applications of the low-grade bauxite in the refractory industry, a calcination integrated with acid leaching method was adopted to remove the potassium (K) and iron (Fe) from the diasporite-illite (DI) type low-grade bauxite. Following calcining the bauxite at different temperatures, the leaching parameters, including the sulfuric acid concentration, temperature, sulfuric acid to bauxite ratio, and reaction time were systematically studied. The appropriate and economical conditions for removing the impurities were found to be calcining the bauxite at 550 °C, and leaching it with a sulfuric acid solution of 1.2 mol/L, sulfuric acid/bauxite ratio of 9 mL/g at a reaction temperature of 70 °C and reaction time of 2 h, under these conditions, the removal efficiency of K and Fe from the bauxite can reach 30.32% and 47.33%, respectively. The treated bauxite was examined by XRD analysis, SEM observations, and chemical analysis. Kinetics of the removing process were calculated by two models, and the results showed that the leaching process was controlled by the mixed shrinking core model, which was affected by both the diffusion through solid layer and the interface transfer. In summary, the approach in this work presents a promising process for comprehensive utilization of the low-grade bauxite.

Keywords: low-grade bauxite; potassium and iron removal; calcination; acid leaching; kinetics

1. Introduction

Bauxite is an important raw material for the alumina industry, from which more than 90% of the world's alumina is produced [1]. With the rapid development of the alumina industry, all bauxite-required industries are confronted with the serious shortage of high-quality bauxite resources. Additionally, China, as a large producer and consumer of alumina, has to import a large amount of bauxite each year from other countries like Australia, Guinea, etc. [2,3]. The bauxite found in China, with the mineral feature of diasporite, characterized by high-aluminum, high-silicon, and low ratio of Al₂O₃/SiO₂ (Al/Si), is an important raw material for the refractory industry and a strategic resource [4]. High-alumina refractory (HAR) extensive applications in the domestic high-temperature industry such as the metallurgical, ceramic, and glass industries, and also retains a great market share in the international market [5].

Compared with the aluminum industry, the scale of refractory industry is smaller. As a raw material, the consumption of bauxite in the refractory industry is less than that in the aluminum industry. This brings a consequence that the majority of bauxite resources are owned by alumina

manufactures, and the refractory companies barely have their own bauxite mines [6]. In recent years, the ore-dressing Bayer process, intensified sintering process, and roasting pretreatment for desulphurization process was developed [7–9], following the technology advances in the industry, the Al/Si ratio requirement in Bayer process can be reduced to 4–5, and a large amount of middle-low grade bauxite is being used. Consequently, the extreme shortage of high-alumina bauxite is found in the refractory industry. In addition, there are more mineral processing researches for alumina industry than the refractory. A great number of studies in the literature on the floatation desilicication, desulfurization, and synthesizing mineral processing agents that serve the aluminum industry [10]. However, very few studies report on the purification of bauxite from the refractory point-of-view.

To balance the usage of bauxite resources in the two industries and ensure their sustainable developments, it has been suggested by Zhong [11] that the beneficiation and purification should be carried out on the bauxite with low ratio of Al/Si and high content of impurity by the refractory producers.

The high-temperature behavior of HAR is based on the mullite ($3\text{Al}_2\text{O}_3 \cdot 2\text{SiO}_2$) phase, which results from the transformation of kaolinite during the high-temperature thermal cycle [12]. In the bauxite, the main impurities that reduce the performance of refractories include Fe_2O_3 , TiO_2 , and R_2O (where $\text{R} = \text{K}$ or Na). These impurities prevent the formation of the mullite and corundum phase [13,14]. It has been found that these impurities form an amorphous phase in the microstructure and that a liquid phase appears easily under high temperature that causes a volume expansion [15]. This leads to degradation of the high-temperature behavior and reduced service life. R_2O almost always forms an amorphous phase and degrades the material properties. Therefore, it is essential to remove the impurities to meet the material requirements for refractory.

There are many methods for iron removal or extraction process from bauxite. Reddy et al. [16] studied the removal of iron from a low grade gibbsitic bauxite with hydrochloric acid and it was found 98% of iron could be removed using 4 mol/L acid. Zhao et al. [17] investigated the dissolution of iron from high iron bauxite from Guangxi province by sulfuric acid. Results showed that the quantity of iron leached was 98.68% with acid concentration of 20% and leaching temperature of 100 °C. Hu et al. [18] developed the direct reduction process for utilization of ferric bauxite. The pretreatment used coal as a reductant, then iron powder was obtained by magnetic separation. Papassiopi et al. [19] proposed an innovative process removing iron from bauxite by iron-reducing bacteria. It was found that 95% of amorphous ferrihydrite could be dissolved, whereas the removal efficiency of goethite and hematite was lower than 9% and 1.2%, respectively. Ma [20] adopted active roasting-acid leaching (HCl) to remove iron and potassium from the bauxite tailing, and the Fe_2O_3 content in the tailing could be decreased to 0.7%, but only 19.2% of K_2O was leached.

However, the removal of potassium in the bauxite has not yet been reported. Since the bauxite studied in this paper is DI type [21] low grade bauxite originating from Dengfeng area, Henan province, and the potassium mainly exists in the illite, the technologies of extracting the potassium from potassium-rich minerals in agriculture can be adopted. There are many relevant studies in this field, including the potassium extraction from mica, nepheline, potassium feldspar, and other potassium-bearing minerals [22–24]. The methods cover soda-sintering, hydrothermal, and acid-leaching technique. Nevertheless, the K_2O content in illite varies from 6% to 9% for agriculture, and it has not reached the industrial requirements ($\text{K}_2\text{O} > 9\%$) [25]. As a result, the extraction of potassium from illite was barely reported.

The objective of this research was to remove iron (Fe) and potassium (K) in low-grade bauxite simultaneously, and a calcination integrated with acid leaching method was adopted. The effects of calcination temperature, sulfuric acid concentration, leaching temperature, sulfuric acid to bauxite ratio, and reaction time on the removal efficiency were studied, and the associated kinetic process was investigated as well. XRD analysis and SEM observations were examined. This study can improve the quality of low -rade bauxite resources and provide better raw materials for the refractory industry.

2. Materials and Methods

2.1. Materials

The bauxite mineral sample used in this work was sourced from Dengfeng, Henan Province, China. Sulfuric acid (H_2SO_4) used as leaching agent is of analytical grade (provided by Aladdin Biotech Shares in Shanghai, China), and all the solutions with specified concentrations were prepared with deionized water.

2.2. Experimental Procedure

The schematic diagram of removing potassium and iron from bauxite is plotted in Figure 1. As described in Figure 1, the bauxite is crushed and milled, and then a muffle furnace was employed to calcine the bauxite at different temperatures (450, 550, 650, 750, 850, 950, 1050, 1250 °C) in air atmosphere. After calcination, the sintered specimens were cooled down to room temperature by air and then ground in a planetary ball mill for 4 h.

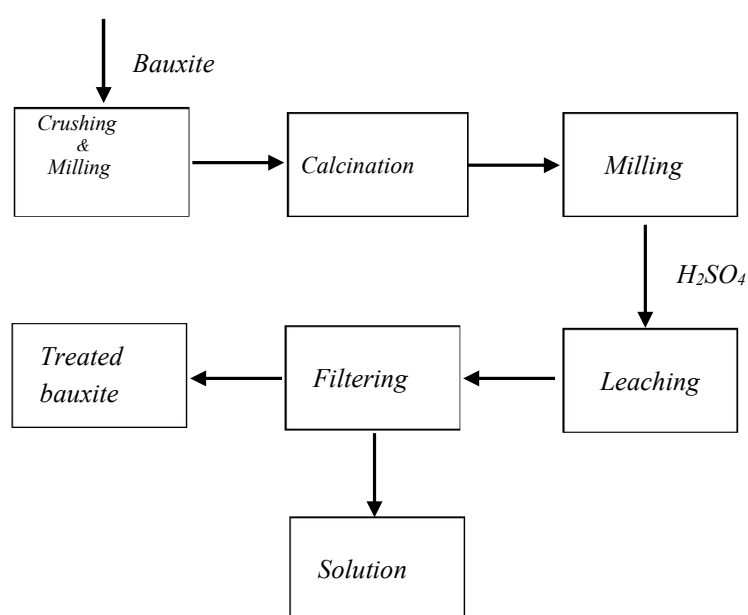


Figure 1. Schematic diagram of removing impurities from bauxite.

Dilute sulfuric acid (H_2SO_4) solutions used for leaching were prepared with deionized water. The leaching experiments were conducted in a 100 mL conical flask in the water bath having a digital temperature controller unit with an accuracy of ± 0.5 °C. Also, the experimental device was equipped with a magnetic stirrer with an agitation speed of 300 rpm and a reflux condenser to avoid mass loss resulting from evaporation. A certain amount of specified sulfuric acid solution was input the glass reactor. When it was heated up to the defined temperature, the roasted bauxite (5 g) was added into the flask with constant stirring (300 rpm). After the desired reaction time, the leaching slurry was immediately filtered through 0.5 μ m pore size white filter paper using a vacuum filtration unit and washed three times to separate the leached product and the solution. The leach liquor was diluted with deionized water to detect the element content of K and Fe. The filter residue was collected, dried, and then characterized.

2.3. Analyzing and Characterizing Methods

The K and Fe content were analyzed by atomic absorption spectrophotometer (AAS, 4530F, Shanghai Precision and Scientific Instrument Co., Ltd., Shanghai, China). The removal efficiency (E_r) was calculated by the Equation (1):

$$E_r = \frac{C_m \times V_l}{M_0} \times 100\% \quad (1)$$

where C_m , V_l , and M_0 represent the concentration of ions (Potassium or Iron) in the leachate (mg/L), leachate volume(L), mass of element (mg) in the ore, respectively. The chemical analysis of the bauxite was performed by X-ray fluorescence (XRF, Rigaku ZSX Primus II, Tokyo, Japan). X-ray diffraction (XRD) patterns of the solid samples were recorded by a Rigaku D/max-rA diffractometer with $\text{CuK}\alpha$ radiation (40 kV and 100 mA). Data points were acquired in the 2θ range of 3 to 70° , with a step size of 0.02° . Thermogravimetric (TG) and differential scanning calorimetry (DSC) analysis were performed by the simultaneous thermal analyzer (NETZSCH 449F3, Selb, Germany) at heating rate of $10^\circ\text{C}/\text{min}$ with a temperature range of 20–1200 $^\circ\text{C}$ in air atmosphere. The morphology of the solid samples was observed using the scanning electron microscopy (SEM, JSM-7500F, JEOL, Tokyo, Japan) equipped with an energy dispersive spectrometer (EDS). The particle distribution of the samples in aqueous solution was observed and analyzed using the optical microscope software (ZEISS Axio Scope. A1, Oberkochen, Germany).

3. Results and Discussion

3.1. Analysis of Raw Material

The chemical analysis performed by XRF indicates that the bauxite consists of 57.34% Al_2O_3 , 18.22% SiO_2 , 3.81% Fe_2O_3 , 3.23% K_2O , 2.32% TiO_2 , 0.26% Na_2O , 0.64% CaO , and 0.23% MgO . The sample with A/S (the Al_2O_3 -to- SiO_2 mass ratio) of 3.15 is low-grade bauxite.

According to the XRD pattern given in Figure 2, the mineral phases in the bauxite are mainly diaspore, quartz and illite. No iron mineral phases are detected in the XRD pattern. As the content of Fe_2O_3 is 3.81 wt % in the raw material, it suggests the possible iron form is that colloidal iron or the substitution—*isomorphous replacement of aluminium atoms by iron atoms in the diaspore and illite crystal lattice.*

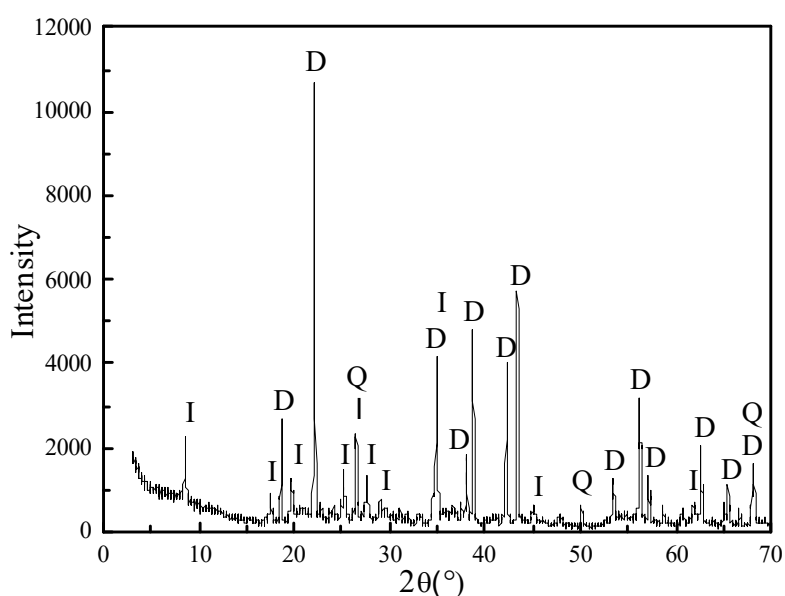


Figure 2. X-ray diffraction (XRD) pattern of the bauxite sample (D, diaspore; Q, quartz; I, illite).

The bauxite is calcined and then ground, and the cumulative particle size is shown in Figure 3, from which it can be seen that approximately 60% of the particles were less than 2 μm , and almost 100% of the particles are less than 20 μm .

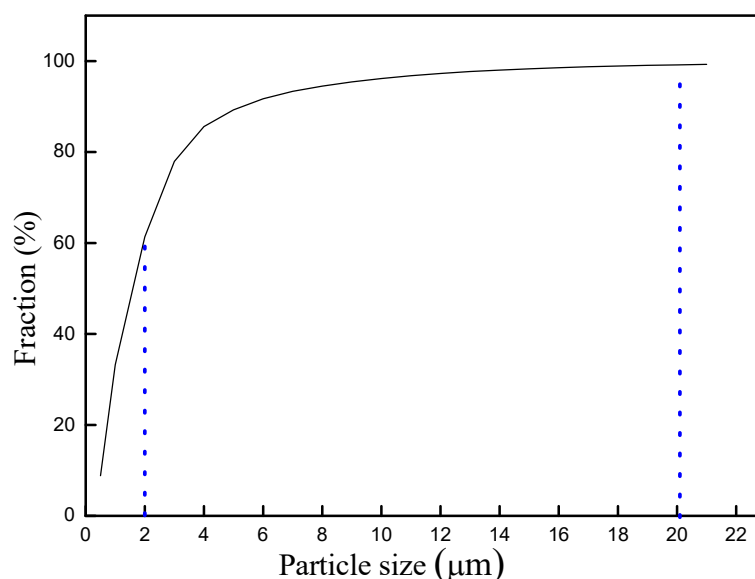
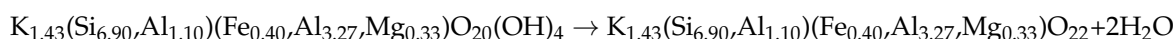
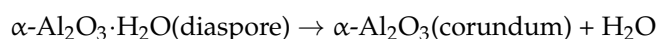


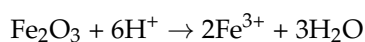
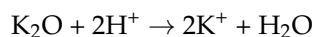
Figure 3. Cumulative particle-size fraction of the bauxite samples.

3.2. Reaction Mechanism

This research was carried out to determine the optimum parameters of removing impurities from bauxite. In the calcination process, the main changes are the phase transformation of diasporite, the dehydroxylation of illite and mullitization. The general crystal chemical formula of illite can be written as $\text{K}_{1.43}(\text{Si}_{6.90}, \text{Al}_{1.10})(\text{Fe}_{0.40}, \text{Al}_{3.27}, \text{Mg}_{0.33})\text{O}_{20}(\text{OH})_4$ [26]. The process can be represented by the following:



In the second step, the release of soluble potassium and iron into solution occurs through the reaction of calcined bauxite with H_2SO_4 . Theoretically, the main chemical reactions during the leaching process can be reflected as follows (written as oxide forms):



3.3. Effect of Calcination Temperature

The thermogravimetric curves of the bauxite are shown in Figure 4. As reported in the literature [27], the sample has an obvious weight loss due to the diasporite dehydroxylation at the temperatures from 490 to 580 $^\circ\text{C}$. Chemically bound water is released from the illite at the temperature from 500 to 700 $^\circ\text{C}$, and the illite is transformed into dehydrate illite (not marked in Figure 4 due to low content). Above 800 $^\circ\text{C}$, the sintering process, vitrification and high-temperature reactions (mullite and corundum formation) take place [28].

From Figure 5, it can be seen that the mineral phase of the bauxite calcined at 450 $^\circ\text{C}$ does not change compared with the raw sample. As the calcination temperature rises, the new phase of corundum ($\alpha\text{-Al}_2\text{O}_3$) appears in the sample, and the diasporite diffraction peaks disappear above 450 $^\circ\text{C}$.

When the temperature rises to 1050 °C, the illite is not observed, and the main phase of the solid sample is corundum due to the high temperature sintering. As reported in [28], above 1100 °C, illite begins to transform into amorphous substance and mullite, while there is no mullite phase discernable in the XRD pattern. The reason for this most likely is that the content of illite is low in the bauxite and only part of illite can transform into mullite.

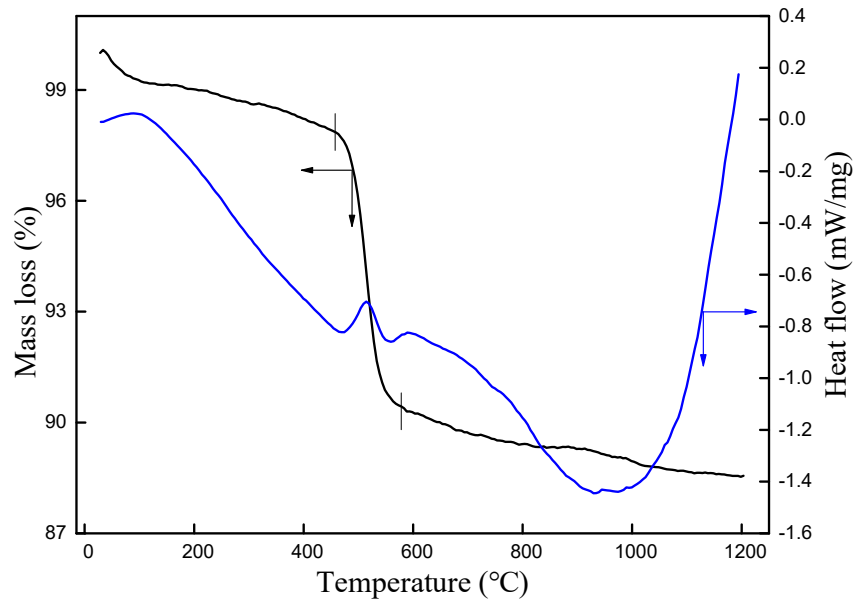


Figure 4. Thermogravimetric (TG) and differential scanning calorimetry (DSC) plots of bauxite sample.

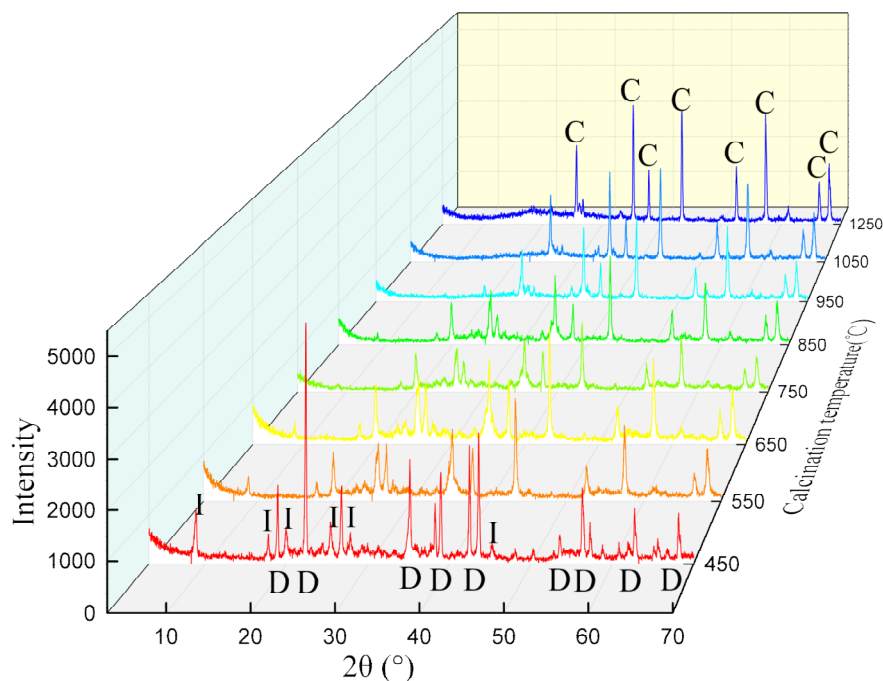


Figure 5. XRD pattern of the bauxite calcined at different temperatures. (D, diaspore. I, illite. C, corundum).

The effect of calcination temperature is studied with leaching in 1.2 mol/L sulfuric acid solution according to the liquid/solid (L/S) of 9 mL/g at a reaction temperature of 70 °C for 2 h, and the results are presented in Figure 6. It can be seen that calcination temperature has a significant effect on removal

efficiency. The removal efficiency of Fe drops sharply from 94.42 to 1.03% when the calcination temperature increases from 450 to 850 °C. Above 850 °C, it keeps below 1.00% until becoming around 0 (not detected) at 1250 °C. The removal efficiency of K increases from 21.46% at 450 °C to 30.32% at 550 °C, reaching the maximum value. Beyond 550 °C, it begins to decrease to approximately 3.00% at 1250 °C.

The phase transformation in Figure 5 can explain the decline of iron removal efficiency as the sintering temperature rises. Specifically, iron enters into the corundum phase and transforms into a solid solution, and the solid solubility of iron in the corundum increases with the increasing temperature. Also, a small portion of iron can form a solid solution ($\text{Fe}_2\text{O}_3 \cdot \text{TiO}_2$) with TiO_2 [29]. Therefore, it is reasonable to deduce that the decrease of iron removal efficiency may be attributed to the transformation of the solid solution at high temperature.

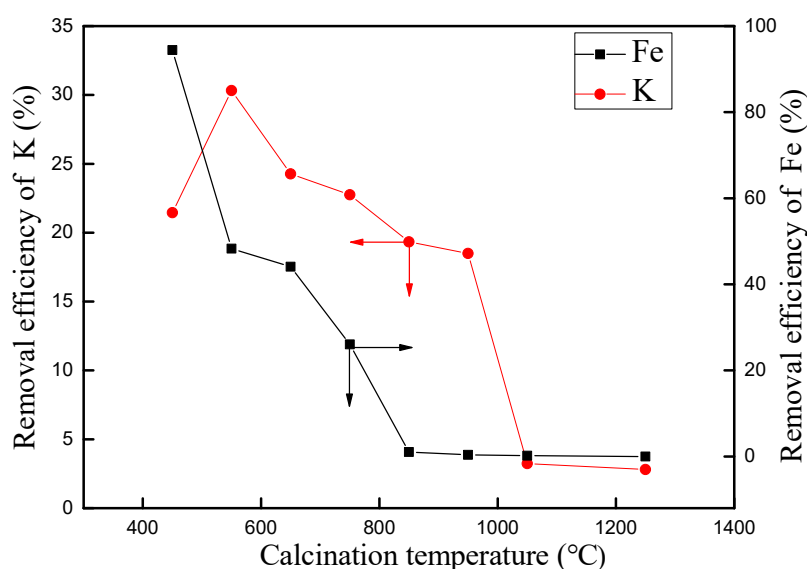


Figure 6. Effect of calcination temperatures on the removal efficiency.

The changes of potassium removal efficiency are mainly associated with the illite crystal structure. As the calcination temperature rises from 450 to 950 °C, the basic charge balance of the illite crystal structure is broken due to the dehydroxylation, causing the adjustment and deformation of the crystal structure. He et al. [30] investigated the crystal structure variation of illite in roasting process. It found that the interplanar distance $d(002)$, $d(004)$, $d(110)$, $d(006)$, $d(131)$, and $d(136)$ of illite increased, and interlayer space expanded along the direction of c -axis, which leads to weakened interlayer force. As a result, the potassium is easily released from the illite, thus we inferred from Figure 5 that the bauxite calcined at 550 °C is advantageous for removing potassium, reaching a maximum value (30.32%). Beyond 550 °C, the illite may transform to a solid solution as the calcination temperature rises, and the potassium removal efficiency begins to decline.

3.4. Leaching Experiment Parameters

From the Figure 6, the removal rate of K reaches the maximal value when the bauxite is roasted at 550 °C, and the rate of Fe is 47.33%. Compared with iron, potassium is more disadvantageous for the refractory performance, so removing potassium is the first consideration. Hence, the roasting temperature is selected to be 550 °C. The leaching experiments are performed to determine the appropriate parameters of removal impurities from the economical view.

3.4.1. Effect of Sulfuric Acid Concentration

A series of experiments are conducted at c (acid concentration) = 0.4, 0.8, 1.2, 1.6, 2.0, 3.0, 4.0 mol/L to investigate the effect of sulfuric acid concentration on removal efficiency. The reaction temperature, liquid/solid ratio and reaction time are kept constant 70 °C, 9 mL/g and 2 h, respectively.

As presented in Figure 7, the removal efficiency of potassium and iron increases gradually with the increasing acid concentration, whose efficiency is raised from 24.71 to 35.54% and 39.71 to 60.78% as the acid concentration is varied from 0.4 mol/L to 4 mol/L, respectively. Higher acid concentration can conduct a strong attack on the minerals and destroy its structure. Besides, for the leaching process, higher acid concentration increases the H^+ activity [31], which may enhance the ion exchange capacity between metal ion and H^+ , resulting in increasing potassium and iron removal efficiency.

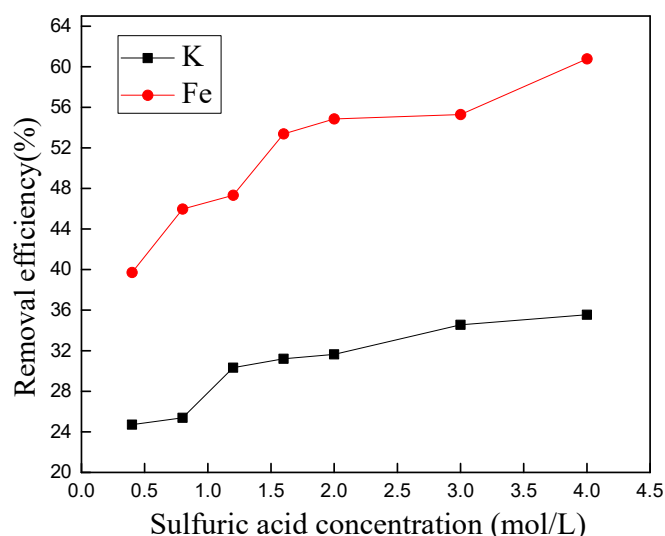


Figure 7. Effect of sulfuric acid concentration on the removal efficiency.

However, the potassium removal efficiency increases slightly from 30.32 to 35.54% as the acid concentration changes from 1.2 to 4 mol/L due to the main potassium-bearing mineral, illite, a layered silicate with relatively stable Al-Si-O tetrahedron crystal structure. Potassium is stably attached to oxygen by ionic bond in the crystal structure, thereby making it difficult for potassium to enter into the solution. Higher acid concentration cannot promote the removal efficiency greatly. Thus, in the following experiments, sulfuric acid concentration is kept at 1.2 mol/L.

3.4.2. Effect of Reaction Temperature

The relationship between the reaction temperature (from 30 to 90 °C) and the removal efficiency was investigated with sulfuric acid concentration of 1.2 mol/L, liquid/solid of 9 mL/g and reaction time of 2 h. The results are illustrated in Figure 8. As expected, rising temperature is favorable for the removal efficiency of potassium and iron. The efficiency of K and Fe removal is as high as 33.74% and 57.95% at 90 °C, respectively. Higher temperature can increase the diffusion coefficient of the reaction system and enhance the diffusion of H^+ from the surface into the inside channels of the mineral particles, accelerating the decomposition of bauxite. Other similar experiments [24] like extraction of potassium from phosphorus-potassium associated ore affirmed that rising the reaction temperature can increase the leaching efficiency. However, higher temperature may cause an Al loss from the bauxite, which is disadvantageous considering the relationship between Al content and refractory performance. Therefore, the appropriate temperature of 70 °C is recommended in this study.

3.4.3. Effect of Sulfuric Acid/Bauxite Ratio

To observe the effect of liquid/solid ratio on the removal efficiency, the experiments were carried out with four ratio levels ranging from 5 to 11 mL/g at acid concentration of 1.2 mol/L, 70 °C for 2 h. The results plotted in Figure 9 showed that the removal efficiency of K and Fe increases with the increase of the sulfuric acid-to-bauxite ratio. This can be explained that higher acid/bauxite ratio supplies more sulfuric acid to leach the potassium and iron. In addition, higher ratio can reduce reaction system viscosity of reactants for improving well mixing and promote diffusion. When the ratio varies from 5 to 11 mL/g, the removal efficiency of potassium and iron only increases from 24.12% to 31.14% and 37.55% to 50.26%, respectively, which does not obviously increase the extent of removing. This reveals that the amount of sulfuric acid is adequate to leach potassium and iron when the ratio exceeds 7 mL/g. Taking the lower acid concentration (1.2 mol/L) into account, the ratio of 9 mL/g is found to be the optimum for leaching.

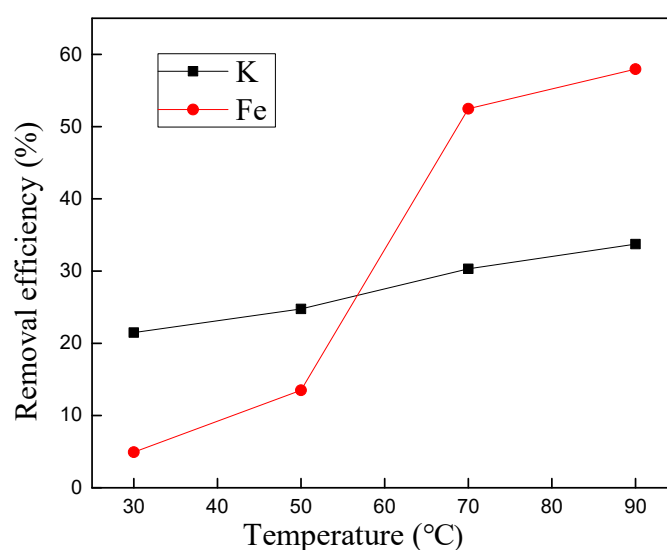


Figure 8. Effect of temperature on the removal efficiency.

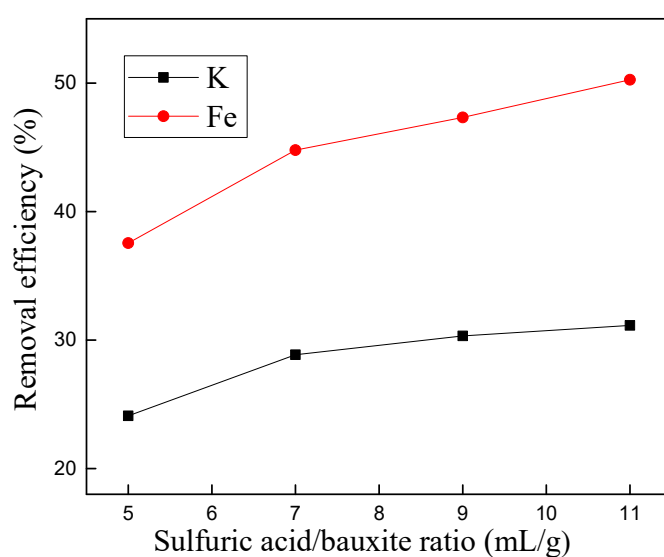


Figure 9. Effect of sulfuric acid/bauxite ratio on the removal efficiency.

3.4.4. Effect of Reaction Time

The effect of the reaction time on the removal efficiency of potassium and iron was studied at 70 °C with sulfuric acid concentration of 1.2 mol/L and liquid/solid ratio of 9 mL/g. The curves reported in Figure 10 identify that the removal efficiency of K and Fe increases with adding time. The efficiency of Fe increases greatly with the increasing time from 25.09% at 20 min to 60.45% at 360 min. Beyond 360 min, the data increases extremely slowly. The removal efficiency of K displays a similar trend, whereas the increasing extent is relatively smaller compared with Fe. This may be due to the different forms of iron present in the bauxite.

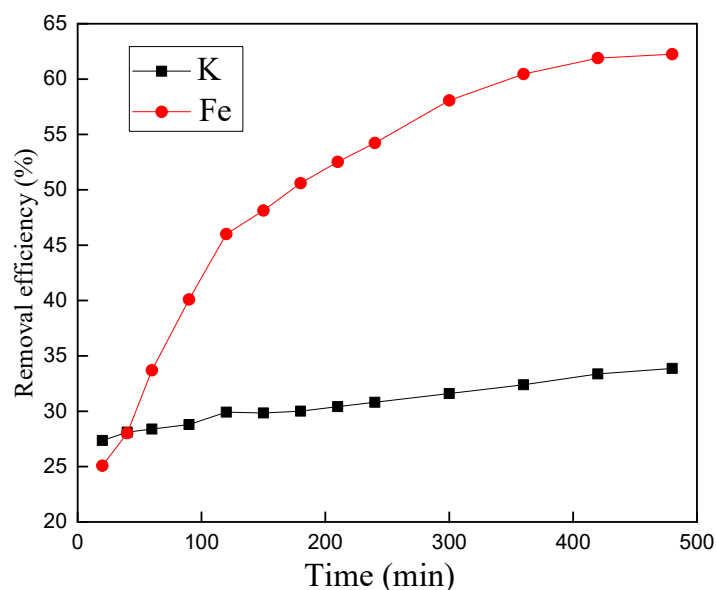


Figure 10. Effect of reaction time on the removal efficiency.

As shown in Figure 10, the removal efficiency of K increases quite slowly as the time increases, for the sake of energy consumption, reaction time of 2 h is chosen as the appropriate condition for the leaching process.

3.5. Kinetics Analysis

The kinetics of removing potassium and iron process were examined at acid concentration of 1.2 mol/L, 70 °C, and L/S of 9 mL/g. The experimental data was analyzed based on the diffusion shrinking core model (SCM). Generally, the diffusion through solid layer and the mixed shrinking core model (diffusion through solid layer integrated with interface transfer) could be the most likely rate-controlling step during the leaching process. The rate equation for diffusion through solid layer and the mixed shrinking core model can be respectively expressed as Equation (2) and Equation (3) [32,33].

$$1 + 2(1 - \alpha) - 3(1 - \alpha)^{\frac{2}{3}} = k_1 \times t \quad (2)$$

$$\frac{1}{3} \ln(1 - \alpha) + (1 - \alpha)^{-\frac{1}{3}} - 1 = k_2 \times t \quad (3)$$

where α is the removal efficiency of potassium or iron, k_1 and k_2 are the linear rate constants controlled by diffusion through solid layer and the mixed shrinking core model, and t is the reaction time in minutes.

The experimental data of Figure 10 are simulated, and the plots of Equations (2) and (3) versus time are presented in Figures 11 and 12, respectively. It can be found from Figure 12 that Equation (3) can better describe the leaching process of potassium and iron because the data in Figure 12 are linear

with a higher correlation coefficients (R^2) compared to Figure 11. The results indicate that the kinetics of the removal of potassium and iron in sulfuric acid is controlled by both the diffusion through solid layer and interface transfer. The rate constant (k_2) and intercept are obtained from Figure 12, and the kinetics models for removing potassium and iron are respectively concluded by Equations (4) and (5).

$$\frac{1}{3} \ln(1 - \alpha) + (1 - \alpha)^{-\frac{1}{3}} - 1 = 8.284 \times 10^{-6} \times t + 0.00593 \quad (4)$$

$$\frac{1}{3} \ln(1 - \alpha) + (1 - \alpha)^{-\frac{1}{3}} - 1 = 1.382 \times 10^{-4} \times t + 0.00332 \quad (5)$$

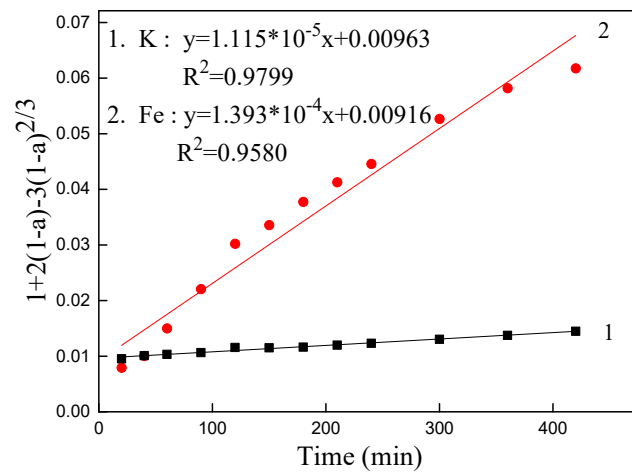


Figure 11. The diffusion kinetics model during removing process: $1 + 2(1 - \alpha) - 3(1 - \alpha)^{2/3}$ versus reaction time.

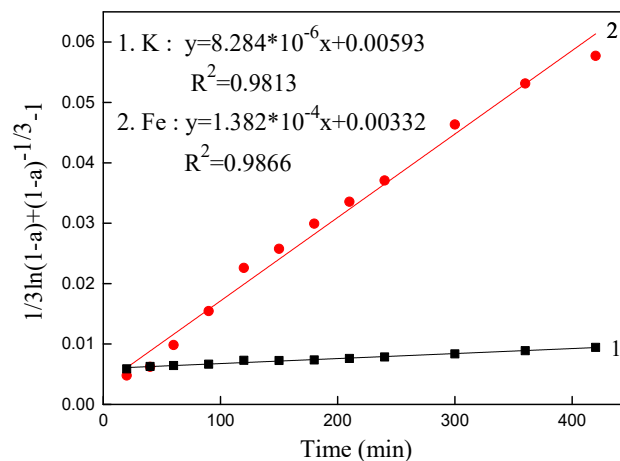


Figure 12. The diffusion kinetics model during removing process: $\frac{1}{3} \ln(1 - \alpha) + (1 - \alpha)^{-1/3} - 1$ versus reaction time.

3.6. Characterization of Treated Bauxite

The XRD patterns of the roasted bauxites and the leach residues are observed in Figure 13. It can be seen that a, b and c have the same crystal phases with illite and corundum. The XRD results indicated that the illite in the bauxite has a very stable crystal structure, which was not destroyed even by the 4 mol/L sulfuric acid attack. The stable crystal structure should be responsible for the lower potassium removal efficiency.

The SEM images and corresponding EDS analysis of the roasted bauxite and the leaching residue H_2SO_4 are obtained in Figure 14. The fuzzy particle boundary and dendritic shape could be observed in Figure 14a, while in Figure 14b, the dendritic shape disappeared due to acid leaching, and it presents different shapes and irregular particles of roughly $0.5\text{--}1\ \mu\text{m}$ in length after leaching. There are no obvious layer shapes of illite in the SEM images, though the illite phase is identified in Figure 13. We can deduce that it may be encapsulated into the transformation product (corundum), and the iron-bearing mineral maybe encountered the similar situation.

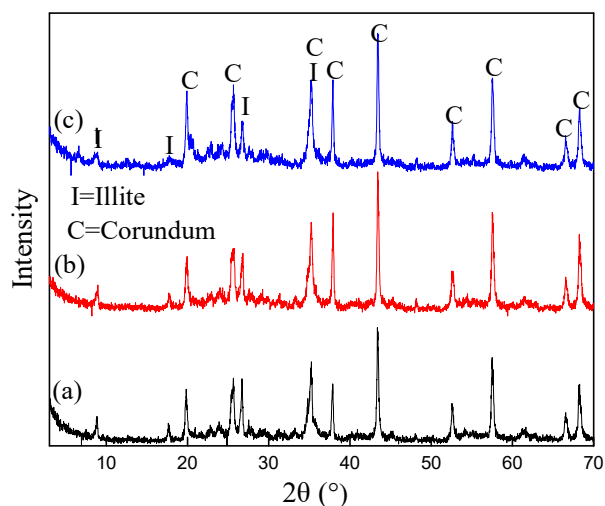


Figure 13. The XRD patterns of treated bauxites ((a): bauxite roasted at $550\ ^\circ\text{C}$. (b): leached with $1.2\ \text{mol/L}\ H_2SO_4$, (c): leached with $4\ \text{mol/L}\ H_2SO_4$).

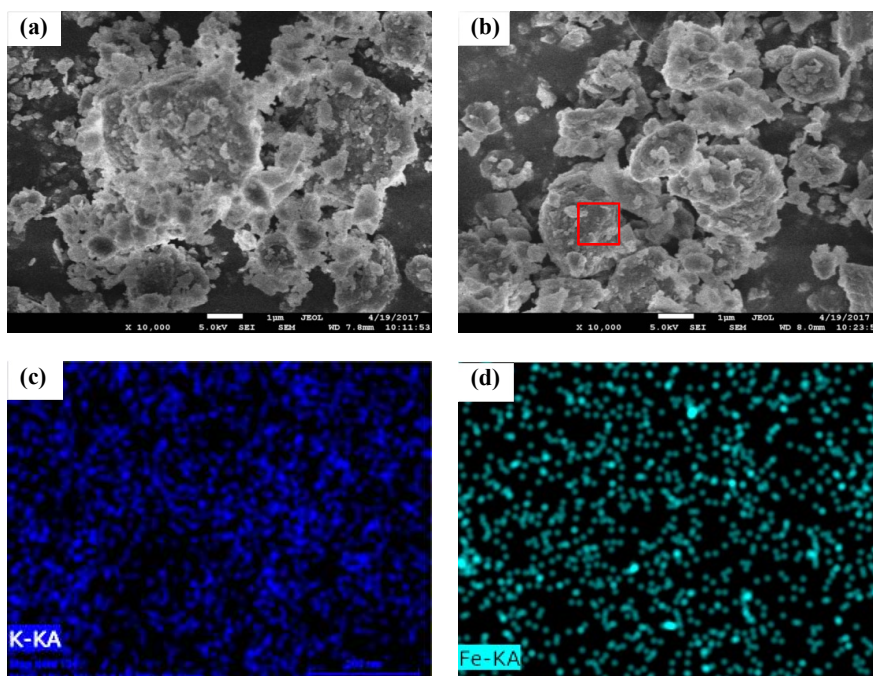


Figure 14. Scanning electron microscopy (SEM) images and energy dispersive spectrometer (EDS) analysis of the treated bauxite. (a): Bauxite roasted at $550\ ^\circ\text{C}$; (b): leaching residue; (c) and (d): EDS analysis for assigned zone.

The combined EDS analysis results in Figure 14c illustrates there are still quantities of K and Fe distribution in the residue, which also suggests the mineral embedded characteristics are complex and it is difficult to remove the impurities.

The chemical analysis of the treated and raw bauxite is presented in Table 1. The equivalent content of K_2O and Fe_2O_3 reduces to 2.09 and 1.78%, respectively. The treated bauxite with relatively low impurities (about 2% of R_2O) can be used to produce homogenized bauxite [34]. Notably, the content of Al_2O_3 is not decreased after leached, which is advantageous for the use in refractory applications.

Table 1. The X-ray fluorescence (XRF) results of bauxite samples, presented as oxides.

Sample	Al_2O_3 (%)	SiO_2 (%)	TiO_2 (%)	Fe_2O_3 (%)	K_2O (%)	Na_2O (%)	CaO (%)	MgO (%)
Treated	58.17	20.56	1.82	1.78	2.09	0.07	0.09	0.15
Raw	57.34	18.22	2.32	3.81	3.23	0.26	0.64	0.23

4. Conclusions

In order to explore a method to apply low-grade bauxite in the refractory industry, a calcination followed by acid leaching process for the impurity removal of low-grade bauxite is proposed. Sulfuric acid is used as a leaching agent in this work. The results prove that raising the calcination temperature is disadvantageous for removing iron, but the removal efficiency of potassium can reach its maximum value when the calcination temperature is 550 °C. The influencing factors including acid concentration, temperature, sulfuric acid-to-bauxite ratio, and reaction time are investigated. It is found that when a sulfuric acid (1.2 mol/L) to bauxite ratio of 9 mL/g and a temperature of 70 °C and a residence time of 2 h are used, the potassium- and iron-removing efficiency from the bauxite calcined at 550 °C can reach 30.32% and 47.33%, respectively, and the treated bauxite can be used to produce homogenized bauxite. The kinetics formulas are calculated, and the results showed that the leaching reaction is controlled by both the diffusion through solid layer and interface transfer. In summary, this research provides prospects for a more comprehensive utilization of low-grade bauxite.

Acknowledgments: The financial support from the National Nature Science Foundation of China (No. U1704252 and 51704263) is gratefully acknowledged. We also thank the Development Fund for Outstanding Young Teachers of Zhengzhou University (No. 1421324065) and the China Postdoctoral Science Foundation (No. 2017M622375).

Author Contributions: Zhuang Li, Yijun Cao, and Yuanli Jiang conceived and designed the experiments; Zhuang Li, Guixia Fan, and Guihong Han performed the experiments; Luping Chang, Guihong Han, and Zhuang Li analyzed the data; Luping Chang and Guixia Fan contributed reagents, materials, and analysis tools; Zhuang Li, Yijun Cao, and Yuanli Jiang wrote the paper.

Conflicts of Interest: The authors declare no conflict of interest.

References

- Paz, S.P.A.; Angélica, R.S.; Kahn, H. Optimization of the reactive silica quantification method applied to Paragominas-type gibbsitic bauxites. *Int. J. Miner. Process.* **2017**, *162*, 10–15. [[CrossRef](#)]
- Zhang, B.; Jiang, Y.; Guo, S.; Zhou, F. The influence of bauxite resource change in China on layout of world alumina industry. *Light Met.* **2014**, *26*, 1–5.
- Fan, Z.L.; Ma, Z.H. Countermeasures and safety evaluation on the use of foreign bauxite resources. *China Min. Mag.* **2010**, *19*, 13–15.
- Zhong, H.; Liu, G.Y.; Xia, L.Y.; Lu, Y.P.; Hu, Y.H.; Zhao, S.G.; Yu, X.Y. Flotation separation of diasporite from kaolinite, pyrophyllite and illite using three cationic collectors. *Miner. Eng.* **2008**, *21*, 1055–1061.
- Pan, S.X.; Wang, R.; Zhang, Z.Q.; Chu, G.S.; Wang, T.Z. Export and import situation of refractories and refractory raw materials in China. *China Refract.* **2000**, *3*, 11–15.
- Shi, G. Discussion on current situation of China's refractories resources and development. *Naihuo Cailiao* **2007**, *41*, 63–67.
- Fang, C.J.; Chang, Z.Y.; Feng, Q.M.; Xiao, W.; Yu, S.C.; Qiu, G.Z.; Wang, J. The Influence of Backwater Al^{3+} on Diasporite Bauxite Flotation. *Minerals* **2017**, *7*, 195.

8. Li, X.B.; Liu, X.M.; Liu, G.H.; Peng, Z.H.; Liu, Y.X. Study and application of intensified sintering process for alumina production. *Chin. J. Nonferr. Met.* **2004**, *14*, 1031–1036.
9. Lü, G.Z.; Zhang, T.A.; Li, B.; Dou, Z.H.; Zhang, W.G. Roasting Pretreatment of High-sulfur Bauxite. *Chin. J. Process. Eng.* **2008**, *8*, 892–896.
10. Zhao, Q.; Miller, J.D.; Wang, X.M. Recent Developments in the Beneficiation of Chinese Bauxite. *Miner. Process. Extr. Metall. Rev.* **2010**, *31*, 111–119.
11. Zhong, X.C. Strategic thoughts on innovative development of Chinese bauxites. *Naihuo Cailiao* **2009**, *43*, 241–243.
12. Amrane, B.; Ouedraogo, E.; Mamen, B.; Djaknoun, S.; Mesrati, N. Experimental study of the thermo-mechanical behaviour of alumina-silicate refractory materials based on a mixture of Algerian kaolinitic clays. *Ceram. Int.* **2011**, *37*, 3217–3227. [[CrossRef](#)]
13. Cheng, H. Influence of K₂O on Sintering-Synthesizing Mullite with Bauxite. *Chin. Ceram.* **2013**, *49*, 48–50.
14. Sadik, C.; Amrani, I.E.; Albizane, A. Recent advances in silica-alumina refractory: A review. *J. Asian Ceram. Soc.* **2014**, *2*, 83–96. [[CrossRef](#)]
15. Stjernberg, J.; Ion, J.C.; Antti, M.L.; Nordin, L.O.; Lindblom, B.; Odén, M. Extended studies of degradation mechanisms in the refractory lining of a rotary kiln for iron ore pellet production. *J. Eur. Ceram. Soc.* **2012**, *32*, 1519–1528. [[CrossRef](#)]
16. Reddy, B.R.; Mishra, S.K.; Banerjee, G.N. Kinetics of leaching of a gibbsitic bauxite with hydrochloric acid. *Hydrometallurgy* **1999**, *51*, 131–138. [[CrossRef](#)]
17. Zhao, A.C.; Zhang, T.A.; Lü, G.Z.; Dou, Z.H. Study on the leaching rules of aluminum and ferrum from high iron bauxite by acid leaching at low temperature. *J. Funct. Mater.* **2012**, *43*, 105–108.
18. Hu, W.T.; Wang, H.J.; Liu, X.W.; Sun, C.Y.; Duan, X.Q. Restraining Sodium Volatilization in the Ferric Bauxite Direct Reduction System. *Minerals* **2016**, *6*, 31. [[CrossRef](#)]
19. Papassiopi, N.; Vaxevanidou, K.; Paspaliaris, I. Effectiveness of iron reducing bacteria for the removal of iron from bauxite ores. *Miner. Eng.* **2010**, *23*, 25–31. [[CrossRef](#)]
20. Ma, D.Y. Preparation of Mullite-Based Complex Refractory from Bauxite Tailings. Ph.D. Thesis, University of Science and Technology Beijing, Beijing, China, 2015.
21. Gao, Z.X.; Li, G.P. On the classification of Chinese bauxites. *J. Chin. Ceram. Soc.* **1984**, *2*, 115–122.
22. Zheng, L.; Yang, Y.; Ma, H.W.; Liu, M.T.; Ma, X. Recovery of magnesium and potassium from biotite by sulfuric acid leaching and alkali precipitation with ammonia. *Hydrometallurgy* **2015**, *157*, 188–193.
23. Yuan, B.; Li, C.; Liang, B.; Lü, L.; Yue, H.R.; Sheng, H.Y.; Ye, L.P.; Xie, H.P. Extraction of potassium from K-feldspar via the CaCl₂ calcination route. *Chin. J. Chem. Eng.* **2015**, *23*, 1557–1564. [[CrossRef](#)]
24. Zhang, Y.F.; Ma, J.Y.; Qin, Y.H.; Zhou, J.F.; Li, Y.; Wu, Z.K.; Wang, T.L.; Wang, W.G.; Wang, C.W. Ultrasound-assisted leaching of potassium from phosphorus-potassium associated ore. *Hydrometallurgy* **2016**, *166*, 237–242. [[CrossRef](#)]
25. Ma, H.W.; Yang, J.; Su, S.Q.; Liu, M.T.; Zheng, H.; Wang, Y.B.; Qi, H.B.; Zhang, P.; Yao, W.G. 20 Years Advances in Preparation of Potassium Salts from Potassic Rocks: A Review. *Acta Geol. Sin-Engl.* **2015**, *89*, 2058–2071.
26. Drits, V.A.; Zviagina, B.B. Trans-vacant and cis-vacant 2:1 layer silicates: Structural features, identification, and occurrence. *Clays Clay Miner.* **2009**, *57*, 405–415. [[CrossRef](#)]
27. Yang, H.M.; Yang, W.G.; Hu, Y.H.; Qiu, G.Z. Kinetics analysis of thermal decomposition reaction of diaspore. *Chin. J. Nonferr. Met.* **2003**, *55*, 9750–9757.
28. Wattanasiriwech, D.; Srijan, K.; Wattanasiriwech, S. Vitrification of illitic clay from Malaysia. *Appl. Clay Sci.* **2009**, *43*, 57–62. [[CrossRef](#)]
29. Wang, J.X.; Zhong, X.C. The effects of potassium oxide and iron oxide additions on the phase composition of sintered bauxites (DK type). *J. Chin. Ceram. Soc.* **1984**, *12*, 77–84.
30. He, D.S.; Feng, Q.M.; Zhang, G.F.; Long, S.S.; Ou, L.M.; Lu, Y.P. Effect of roasting on dissolution behavior of illite in acid solution. *J. Cent. South Univ.* **2011**, *42*, 1533–1537.
31. Bibi, I.; Singh, B.; Silvester, E. Dissolution of illite in saline-acidic solutions at 25 °C. *Geochim. Cosmochim. Acta* **2011**, *75*, 3237–3249. [[CrossRef](#)]
32. Çalban, T.; Kaynarca, B.; Kuşlu, S.; Çolak, S. Leaching kinetics of Chevreul's salt in hydrochloric acid solutions. *J. Ind. Eng. Chem.* **2014**, *20*, 1141–1147. [[CrossRef](#)]

33. Dickinson, C.F.; Heal, G.R. Solid–liquid diffusion controlled rate equations. *Thermochim. Acta* **1999**, *340*, 89–103. [[CrossRef](#)]
34. Lin, B.Y.; Hu, L. *Raw Materials of Refractory*; Metallurgical Industry Press: Beijing, China, 2015; pp. 137–166. ISBN 978-7-5024-7038-8.



© 2018 by the authors. Licensee MDPI, Basel, Switzerland. This article is an open access article distributed under the terms and conditions of the Creative Commons Attribution (CC BY) license (<http://creativecommons.org/licenses/by/4.0/>).